Experimental Implementation of Wave Propagation in Disordered Time-Varying Media

Benjamin Apffel,[1,2] Sander Wildeman,[1,2] Antonin Eddi,[2] and Emmanuel Fort[1,*]
[1]Institut Langevin, ESPCI Paris, Université PSL, CNRS, Institut Langevin, 1 rue Jussieu, F-75005 Paris, France
[2]PMMH, CNRS, ESPCI Paris, Université PSL, Sorbonne Université, Université de Paris, F-75005 Paris, France

(Received 15 February 2021; accepted 11 February 2022; published 4 March 2022)

Here, we study and implement the temporal analog in time disordered sytems. A spatially homogeneous medium is endowed with a time structure composed of randomly distributed temporal interfaces. This is achieved through electrostriction between water surface and an electrode. The wave field observed is the result of the interferences between reflected and refracted waves on the interfaces. Although no eigenmode can be associated with the wave field, several common features between space and time emerge. The waves grow exponentially depending on the disorder level in agreement with a 2D matrix evolution model such as in the spatial case. The relative position of the momentum gap appearing in the time modulated systems plays a central role in the wave field evolution. When tuning the excitation to compensate for the damping, transient waves, localized in time, appear on the liquid surface. They result from a particular history of the multiple interferences produced by a specific sequence of time boundaries.

DOI: 10.1103/PhysRevLett.128.094503

Spatial disorder induces significant changes in wave propagation. Localization and wave focusing are observed in many contexts [1] such as in quantum [2–5], optical [6–8], acoustic [9], seismic [10], or hydrodynamic [11–13] systems. When waves travel through a spatially disordered medium interferences between counterpropagating waves result in enhanced backscattering and weak localization [6,14] at low disorder and Anderson localization [2,7] for higher disorder.

Because time and space are, to some extent, interchangeable in wave propagation, several phenomena observed in spatially modulated systems have a temporal counterpart in the time modulated ones [15–22]. Dynamical localization have been previously studied in the momentum space with quantum "kicked rotor" systems [23,24] or with quantum particles confined spatially in a time varying potential through a theoretical approach [25,26]. These systems are modulated by a properly disordered pseudoperiodic driving force and are localized in space and periodic in time. The dynamic of these disordered systems is described by the first derivative of the wave function given by the Schrödinger equation and lead to localization in impulsion.

Here, we focus on waves governed by a wave equation with a second derivative in time, such as Maxwell's equations, propagating in a spatially homogeneous medium with disordered time varying properties. Such systems have been studied theoretically very recently [27–29] identifying universal statistics like exponential growth of the wave energy. We implement experimentally this system with water waves propagating in a medium submitted to a series of disordered time interfaces actuated electrically. First, we introduce a simple model of this system. We then show and discuss the experimental results.

Our model is based on a spatially invariant system submitted to a temporal modulation of its propagation properties in the form of a Dirac comb with a controlled level of time disorder. The Dirac comb is a standard model used for spatially periodic potentials in which a modulated potential is replaced with discrete boundary conditions [30]. Figure 1(a) shows a schematics of a wave front propagating in a 1D Dirac comb potential with the multiple reflections and transmissions at each interface. Figure 1(b) shows the time analog with the Dirac comb composed of time interfaces induced by the periodic forcing. The time reflections and transmissions on the interfaces generate counterpropagating and copropagating waves, respectively [31,32]. In both cases, the wave field results from interferences between multiple waves generated at the interfaces.

We use liquids to study the effect of disorder in time modulated systems. Large amplitude and versatile time modulations can be easily implemented in liquids [31–35]. A time interface was obtained by applying a sudden vertical jolt. An initial wave propagating on the liquid produced a copropagating and a counterpropagating wave associated to the transmitted and the reflected wave respectively [31]. Here, we use electrostriction to perform time interface. A flat electrode is placed at a distance d above the grounded conductive water surface [36–38]. The electric field exerts an attractive force on the liquid surface modifying the wave speed $c(k)$ for a wave number k as

$$c(k)^2 = c_0^2(k)[1-\alpha(t)] \quad \text{with} \quad \alpha(t) = \chi_0 V(t)^2 \quad \text{and} \quad \chi_0 = \epsilon/[\rho c_0^2(k) d^2 \tanh(kd)]\,. \tag{1}$$

$V(t)$ is the electric potential, c_0 the wave speed for $V(t) = 0$ given by the gravity-capillary dispersion relation, ϵ the dielectric permittivity of the air, and ρ the density of the liquid [36–38]. Electric pulses of maximum amplitude V_0 and duration τ_p at successive discrete times T_n, n being an integer, are modeled as a Dirac comb $V(t)^2 = fV_0^2\tau_p \sum_{n\geq 0} \delta(t - T_n)$ with f accounting for the shape of the pulse. In the experiments, $\chi_0 V_0^2$ is typically of the order of 0.3–0.5. Electrostriction offers extensive experimental possibilities for controlling the temporal properties of a medium with short-time response, huge amplitude variations and the ability to hold these changes over an arbitrary time.

The time evolution of the wave field $\phi(\boldsymbol{k}, t)$ of wave vector $\boldsymbol{k}$ satisfies the nonhomogeneous wave equation [31]

$$\frac{\partial^2\phi}{\partial t^2}(\boldsymbol{k}, t) + 2\Gamma\frac{\partial\phi}{\partial t}(\boldsymbol{k}, t) + \omega_0^2\phi(\boldsymbol{k}, t) = \omega_0^2\beta_0 \sum_{n\geq 0} \delta(t - T_n)\phi(\boldsymbol{k}, t)\,, \tag{2}$$

with $\omega_0 = c_0 k$ the wave angular frequency, $\beta_0 = f\chi_0 V_0^2\tau_p$ and Γ the wave damping rate due to viscosity, $\Gamma = 2\nu k^2$ with ν being the kinematic viscosity of the liquid [39]. This equation is the time counterpart of the Helmholtz equation in k space. In practice, $1/\Gamma \gg \tau_p$. The time interfaces can be interpreted as sources proportional to the wave field $\phi(\boldsymbol{k}, T_n)$ at the time of the electric pulse [31]. We solve Eq. (2) using a matrix transfer approach. The evolution of the wave field is completely characterized by $\Psi = [\phi\ (1/\omega_0)(\partial\phi/\partial t)]^T$. The crossing of the time interface is given by $K = \begin{bmatrix} 1 & 0 \\ \omega_0\beta_0 & 1 \end{bmatrix}$ and the propagation during $\Delta T_n = T_{n+1} - T_n$ between two successive time interfaces is given by $R(\Delta T_n) = e^{-\Gamma\Delta T_n}\begin{bmatrix} \cos(\omega_0\Delta T_n) & \sin(\omega_0\Delta T_n) \\ -\sin(\omega_0\Delta T_n) & \cos(\omega_0\Delta T_n) \end{bmatrix}$.

Thus, the evolution of the wave field satisfies $\Psi_{n+1} = M_n\Psi_n = R(\Delta T_n)K\Psi_n$ which by recurrence gives $\Psi_{n+1} = (\prod_{p\leq n} M_p)\Psi_0$. For a periodic excitation, $\Delta T_n = T$, $M_0 = R(T)K$, and $\Psi_{n+1} = M_0^{n+1}\Psi_0$. Following Floquet analysis, the two eigenvalues of M_0 can be written $\lambda_j = e^{(i\mu_j - \Gamma)T}$ with μ_j a complex value and $j = 1$ or 2. Figure 1(c) shows the real part of $(i\mu_j - \Gamma)T$ (red line) and its imaginary part (blue lines) as a function of k. Vertical momentum k gaps associated with real values of μ_j are visible. They are the analog of energy gaps in spatial crystals. However, while the latter are forbidden admitting only exponentially decaying solutions due to energy conservation, k gaps also allow exponentially increasing

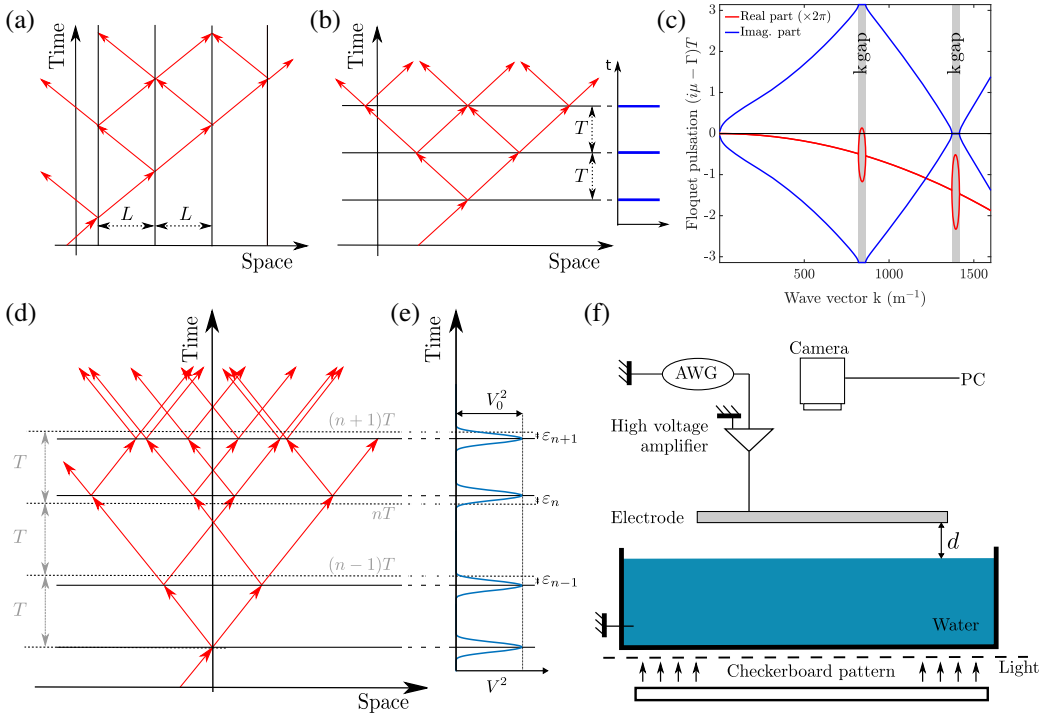

FIG. 1. Schematics of the wave front reflections and transmissions on a spatial Dirac comb (a) and a temporal one (b). (c) Floquet diagram with vertical k gaps for a temporal Dirac comb with damping ($V_0 = 8.0$ kV, $d = 5$ mm, and $2\nu = 7 \times 10^{-6}$ m^2/s). (d) Schematics of the wave front propagation in a temporal Dirac comb with disorder obtained by shifting the time interfaces and (e) associated electric forcing $V(t)^2$. (f) Schematics of the experimental setup with the amplitude wave generator (AWG) controlling the voltage of the electrode.

solutions, as energy can be supplied by the forcing. For $\Re(i\mu_j - \Gamma) > 0$, these solutions lead to the parametric Faraday instability at half the excitation frequency [33–38,40]. It is interesting to note that Eq. (2) is also that of a parametrically excited oscillator [41]. The time evolution of the global wave field is thus identical to the motion of the oscillator under a disordered parametric driving [42,43]. It is thus fully characterized, at a given time, by only to two parameters counterpart of the oscillator position and velocity. For the waves, the multi-interference paths resulting from the splitting at each successive interface [see Fig. 1(b)] is fully characterized by the two Cauchy conditions Ψ at a given time. The contrast with the spatial analog [Fig. 1(a)], which cannot be characterized by only two parameters is probably related to time causality.

We now introduce disorder in the system as a random time shift such that $T_n = (n + \epsilon_n)T$, ϵ_n being a variable taken independently and uniformly in $[-\sqrt{3}\sigma, \sqrt{3}\sigma]$ with σ the disorder standard deviation [see Fig. 1(d)]. The evolution matrices M_n are now random and correlated depending on $\epsilon_{n+1} - \epsilon_n$. However, they can be redefined uncorrelated by setting $\Psi'_n = R(-\epsilon_n T)\Psi_n$ and $M'_n = R(-\epsilon_n T)M_n R(\epsilon_n T)$ to apply the Fürstenberg theorem [44] which states that $\Psi'_n \simeq \exp(\upsilon n)$ for n large enough, with υ being the Lyapunov exponent. This exponential increase should lead to a statistical behavior similar to the one observed in disordered spatial media [45]. A similar exponential behavior has been also observed in the case of parametrically excited oscillators in the presence of noise [42,43].

The experimental setup consists of a $30 \times 30 \times 3$ cm^3 Plexiglas™ container filled with tap water [Fig. 1(e)]. A transparent FTO electrode is suspended horizontally at a distance $d = 5$ mm over the electrically grounded water. The electric potential $V(t)$ consists of narrow peaks of amplitudes V_0 in the range of 6 to 8 kV with a repetition rate of $\omega_0/2\pi = 60$ Hz. The pulses are arch of sinus of duration $\tau_p = 0.4T$ and maximum amplitude V_0 [see Fig. 1(e)]. Matching the integrals $V(t)^2$ to fit the Dirac comb model gives $\beta_0 = (3\tau_p/8)\chi_0 V_0^2$. An electrically induced Faraday instability is triggered above a certain V_0^2 threshold (~8 kV) with waves oscillating at half the forcing frequency $\omega_0/4\pi = 30$ Hz. The wave field is measured from images taken at 90 fps using the deformation of a checkerboard pattern placed below [46]. The amplitude of the Faraday waves $A_F(t)$ at time t is obtained by applying a time filter at $\omega_0/4\pi$ and spatial averaging under the electrode.

We first focus on the effect of disorder on the exponential growth of the wave. Figure 2(a) shows a typical experimental measurement of the time evolution of $A_F(t)$ for various disorder from $\sigma = 0$ to 8.1×10^{-2}. The amplitude of the electric pulses V_0 is set to 7 kV to trigger the Faraday instability. In agreement with the Fürstenberg theorem [44], the wave grows exponentially for small enough amplitudes $[A_F(t) \ll \lambda_F]$ when nonlinear hydrodynamic effects are negligible. These exponential growths of the waves are a statistical signature of the localization in these disordered time varying media [27,28]. The fitted Lyapunov exponents υ (dashed lines) decrease with increasing disorder. A characteristic damping time $1/\Gamma = 0.19$ s is measured from the decay of the Faraday waves when excitation is stopped [see inset Fig. 2(a)]. This value used in the matrix model yields to the Faraday threshold value at $V_0 = 7$ kV which agrees with experiments. From the value of Γ we can extract $2\nu = 7 \times 10^{-6}$ m^2/s that is higher than the expected value for water but of the right order of magnitude [21].

Figure 2(b) shows the fitted exponents υ as a function of the disorder level σ. Each sequence is run three times to ensure that the measured growth rates are robust to experimental drifts. The decrease of υ with increasing σ can be reproduced by the numerical calculations with the

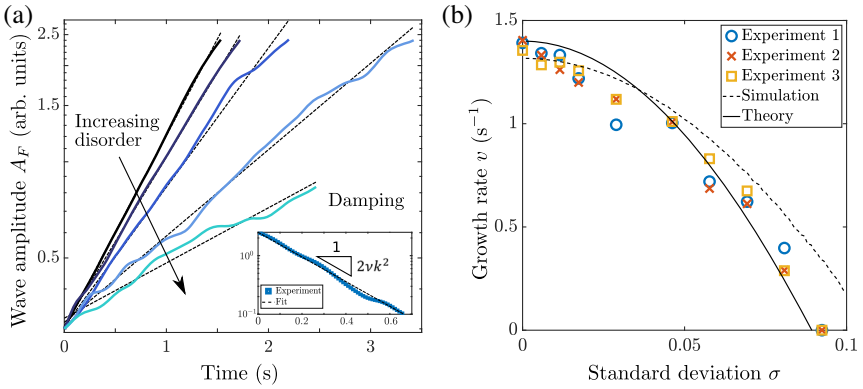

FIG. 2. (a) Growth of the Faraday wave amplitude $A_F(t)$ with time for various disorder levels $\sigma = 0$, 0.017, 0.046, 0.069, and 0.081. The Lyapunov exponents υ are obtained from the exponential fits (dashed lines). Inset: decay of $A_F(t)$ with time when the forcing is turned off. The damping rate Γ is obtained from an exponential fit (dashed line). (b) Fitted Lyapunov exponents υ as a function of σ for various experiments. Numerical simulations from the matrix model (dotted line) taking into account the fitted Γ and theoretical model (full line) based on the decrease of the forcing component at ω_0.

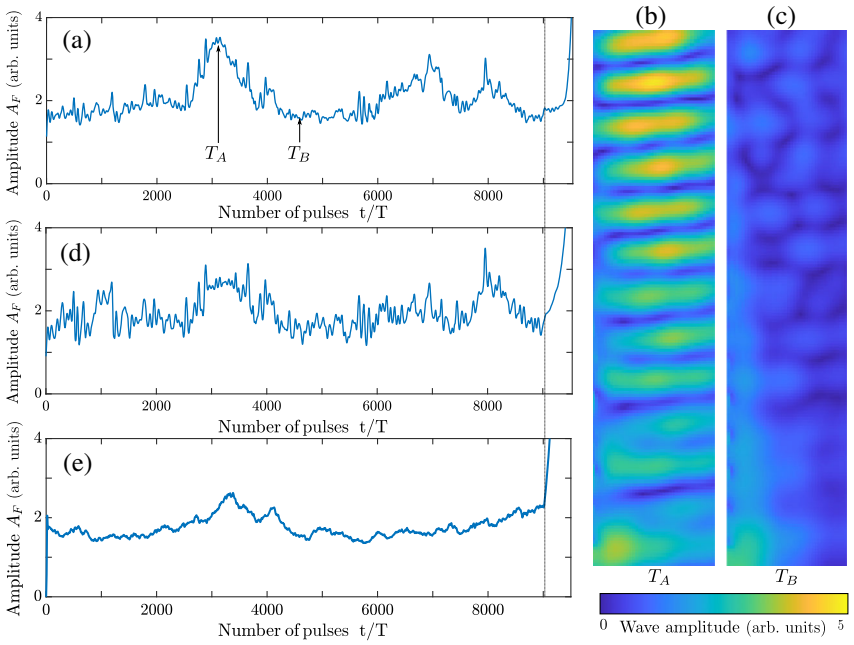

FIG. 3. (a) Time evolution of the Faraday wave amplitude $A_F(t)$ for a periodic excitation with a given disorder sequence with $\sigma = 0.1/\sqrt{3}$. V_0 is tuned at the Faraday instability threshold. The disorder is suppressed at $t > 160$ s (vertical line). (b),(c) Wave fields at the Faraday frequency at time T_A and T_B, respectively. (d) $A_F(t)$ for the same excitation sequence as in (a). (e) Simulated time evolution of $A_F(t)$ using the matrix model for the same excitation sequence as in (a) with $V_0 = 7.322$ kV, $\nu = 7 \times 10^{-6}$ m^2/s, and $d = 5$ mm.

matrix model using the fitted damping rate Γ [see dashed line Fig. 2(b)]. The disorder alters the otherwise perfectly constructive interferences between the reflections and transmissions on the time interfaces. This result can also be interpreted in the spectral domain. Faraday instability is directly related to the oscillation of $V(t)^2$ at ω_0. For small disorder levels, υ is expected to follow $\upsilon(\sigma) \propto [\widehat{V^2}(\sigma) - \widehat{V_F^2}]$, with $\widehat{V^2}(\sigma)$ and $\widehat{V_F^2}$ being the Fourier components of $V^2(t)$ at ω_0 in the presence of disorder and when forcing is set at the Faraday threshold, respectively [47]. From the central limit theorem, one can show that $\widehat{V^2}(\sigma) = \widehat{V^2}(0)\mathrm{sinc}(2\pi\sqrt{3}\sigma) \approx \widehat{V^2}(0)(1 - 2\pi^2\sigma^2)$ for small σ and a large number of pulses. The resulting quadratic shape $\upsilon(\sigma) = \upsilon(0)(1 - \zeta\sigma^2)$ is in good agreement with experimental findings and can be adjusted by setting $\upsilon(0) \approx 1.4$ and $\zeta \approx 120$ [see Fig. 2(b) solid line].

We now focus on the experimental investigation of the amplitude fluctuations of the wave field, which are known to contain significant information on localization processes [48]. Temporal fluctuations of the wave field can be observed experimentally by tuning V_0 at the Faraday threshold for a chosen disorder level σ to achieve a null Lyapunov exponent. The average energy gain induced by the random time interfaces thus compensates for the damping. Figure 3(a) shows the time evolution of the amplitude of the Faraday waves $A_F(t)$ for a given pulse sequence. The periodic excitation with added disorder lasts 160 s. Then, the disorder is removed (vertical line) from the periodic excitation to measure the exponential growth of the wave amplitude. Peaks extending over hundreds of periods T are observed in the Faraday wave amplitude. Figures 3(b) and 3(c)show the wave field at the water surface during and out of a peak. When the same excitation sequence is applied again, the measured wave fluctuations [Fig. 3(d)] are highly correlated in both experiments. This indicates that these fluctuations result from a specific temporal sequence and that the multiwave interference process which produces them is experimentally reproducible. Figure 3(e) shows the simulated fluctuations with the same sequence using the matrix model. Although the correlation is lower, the central double-peak feature is still visible.

The disorder also significantly impacts the waves other than the Faraday mode. Their experimental observation is, however, hindered by the presence of the Faraday waves but numerical simulations make their study possible (setting $\Gamma = 0$, $V_0 = 8.0$ kV, and $d = 5$ mm). We study two modes at the edge of the k gap, just inside ($k_{\mathrm{in}} = 819.5$ m^{-1}) and outside ($k_{\mathrm{out}} = 819.2$ m^{-1}), respectively. The wave amplitude at k_{in} grows exponentially in all cases for various disorder levels in agreement with the model [Fig. 4(a)]. As the disorder level increases, the fitted exponents υ first decrease at low disorder levels ($0 < \sigma < 0.025$) and then increase at higher disorder levels ($\sigma > 0.025$). Outside the k gap, the growth is also exponential but, in this case, the exponent increases monotonously with increasing disorder on the whole σ range,

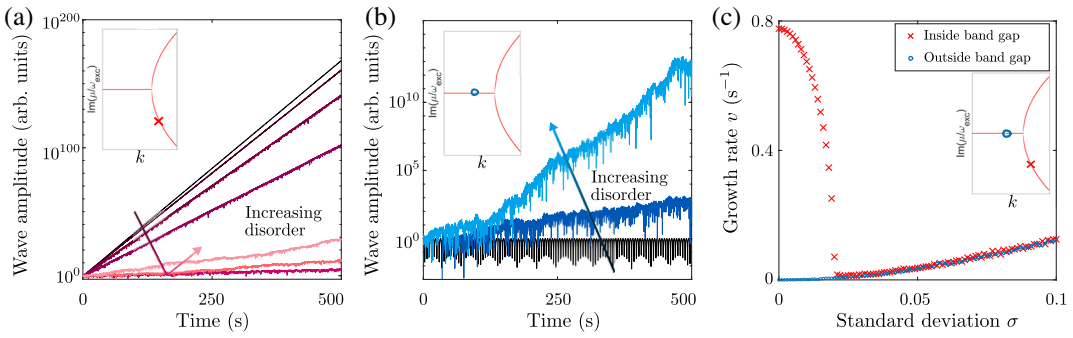

FIG. 4. Simulation of the wave growth with time for different disorder standard deviations for waves (a) just inside and (b) outside the k gap with wave number $k_{\text{in}} = 819.5\ \text{m}^{-1}$ and $k_{\text{out}} = 819.2\ \text{m}^{-1}$, respectively (see insets) and $\sigma = 0.1, 0.6, 1.1, 1.6, 2.1, 7, 10 \times 10^{-2}$ and $\sigma = 0.1, 3, 6 \times 10^{-2}$, respectively. Linear fits (not shown) give the Lyapunov exponents υ. (c) Fitted exponents υ as a function of σ.

$0 < \sigma < 0.1$. The evolution of the exponents υ with σ are plotted in Fig. 4(c) for the two cases k_{in} (red crosses) and k_{out} (blue circles). The two curves superimpose in the regions where υ increases with σ. The decreasing behavior of υ at low disorder levels for k_{in} is similar to the experimental observations at the Faraday frequency [see Figs. 2(a) and 2(b)]. These results are consistent with an effective shrinking of the band gap as the periodicity deteriorates with the disorder. The validity of the Fürstenberg theorem implies that the waves must grow exponentially as observed either inside or outside the gap for arbitrary disorder levels.

Contrary to spatial interfaces, the crossing of a time interface is nonunitary meaning that the energy of the wave field is not conserved across the boundary. From the expression of the matrix K, in the case of a monochromatic wave at ω_0, an incident wave field defined by $\Psi^- = [\phi^- \ (1/\omega_0)(\partial\phi^-/\partial t)]^T$ produces an additional wave field $i\omega_0\beta_0[0 \ (1/\omega_0)(\partial\phi^-/\partial t)]^T$ when crossing the interface (using $\phi^- = i(1/\omega_0)(\partial\phi^-/\partial t)$). Using the superposition principle, this can be written as the sum of a forward propagating wave $(i\omega_0\beta_0/2)[\phi^- \ (1/\omega_0)(\partial\phi^-/\partial t)]^T$ and a time-reversed backward propagating one $-(i\omega_0\beta_0/2)\times [\phi^- \ -(1/\omega_0)(\partial\phi^-/\partial t)]^T$. This interpretation highlights the momentum conservation with the symmetric production of counterpropagative waves as well as the nonconservation of energy with the creation of waves. For an incident wave, the time interface can be characterized by a transmission coefficient $t = 1 + (i\omega_0\beta_0/2)$ and the reflection one $r = -(i\omega_0\beta_0/2)$. The general expression for the incident wave is two counterpropagating waves $\phi^-(\boldsymbol{k}, t) = Ae^{i\boldsymbol{k}\cdot\boldsymbol{r}+i\omega_0 t} + Be^{i\boldsymbol{k}\cdot\boldsymbol{r}-i\omega_0 t}$ with the total energy $E^- \propto |A|^2 + |B|^2$, A, and B being complex values. Just after the boundary, the field becomes $\phi^+(\boldsymbol{k}) = [tA + r^*B]e^{i\boldsymbol{k}\cdot\boldsymbol{r}+i\omega_0 t} + [rA + t^*B]e^{i\boldsymbol{k}\cdot\boldsymbol{r}-i\omega_0 t}$. For an incident propagating wave ($B = 0$), the time interface creates a standing wave with limited amplitude in second order in $\omega_0\beta_0$ ($\Delta E = (\omega_0^2\beta_0^2/2)E^-$). For an incident standing wave, the interface also generates a standing wave with an associated energy $\Delta E \approx (\omega_0\beta_0 \sin\varphi)E^-$ with $B = Ae^{-i\varphi}$. It yields to an energy increase or decay depending on the interference with the incident wave field. To accumulate energy in the time crystal, the phase condition φ must also be recovered after the propagation between two successive interfaces. The relative phase between the two counterpropagative waves must thus change by $2\pi n$, n being an integer between two interfaces. This leads to frequencies $n\omega_0/2$ in the k gaps. The maximum energy output corresponds to the Faraday instability at $\varphi \approx \pi/2$. When moving to the k-gap limits, smaller energy gains are achieved when crossing the time interfaces, reaching zero at the k-gap limit (for $\varphi \approx 0$ or $\pi\varphi$). Note that an associated symmetric overdamped mode exists for the opposite phase [21]. The presence of a random time shift between the interfaces results in fluctuations of the phase-lock condition which in turn changes the energy gain at each interface. For the Faraday mode, since ΔE is maximal, any perturbation results in a decrease of wave growth as observed experimentally [see Fig. 2(b)]. For modes such as k_{in} for which is ΔE not maximal, the output is more complex to infer due to the possible gain or loss of energy resulting from the interplay the perturbed phase shift acquired between two interfaces and the amplitude of ΔE at the crossing of each interface [49].

In summary, time disorder induces temporal wave energy characteristics that are similar to its spatial analog. The exponential growth associated with a Lyapunov exponent not depending on a particular realization of disorder, is somewhat reminiscent of the one-dimensional Anderson localization in space [27,28]. An interesting perspective of these results would be to generalize the effect of disorder on wave propagation with a spatiotemporal disorder and to study the spatiotemporal localization of energy. In addition, this could be implemented experimentally with the use of several electrodes driven independently to realize time-varying inhomogeneous energy landscapes.

The authors would like to thank Rémi Carminati for fruitful discussions. We are thankful for the support of the AXA Research Fund and the French National Research Agency LABEX WIFI (ANR-10-LABX-24).

*Corresponding author.
emmanuel.fort@espci.fr

[1] M. Filoche and S. Mayboroda, Universal mechanism for Anderson and weak localization, Proc. Natl. Acad. Sci. U.S.A. **109**, 14761 (2012).
[2] P. W. Anderson, Absence of diffusion in certain random lattices, Phys. Rev. **109**, 1492 (1958).
[3] G. Modugno, Anderson localization in Bose-Einstein condensates, Rep. Prog. Phys. **73**, 102401 (2010).
[4] J. Billy, V. Josse, Z. Zuo, A. Bernard, B. Hambrecht, P. Lugan, D. Clément, L. Sanchez-Palencia, P. Bouyer, and A. Aspect, Direct observation of Anderson localization of matter waves in a controlled disorder, Nature (London) **453**, 891 (2008).
[5] A. Lubatsch and R. Frank, Self-consistent quantum field theory for the characterization of complex random media by short laser pulses, Phys. Rev. Research **2**, 013324 (2020).
[6] M. P. V. Albada and A. Lagendijk, Observation of Weak Localization of Light in a Random Medium, Phys. Rev. Lett. **55**, 2692 (1985).
[7] M. Segev, Y. Silberberg, and D. N. Christodoulides, Anderson localization of light, Nat. Photonics **7**, 197 (2013).
[8] T. Sperling, W. Bührer, C. M. Aegerter, and G. Maret, Direct determination of the transition to localization of light in three dimensions, Nat. Photonics **7**, 48 (2013).
[9] H. Hu, A. Strybulevych, J. H. Page, S. E. Skipetrov, and B. A. van Tiggelen, Localization of ultrasound in a three-dimensional elastic network, Nat. Phys. **4**, 945 (2008).
[10] E. Larose, L. Margerin, B. A. van Tiggelen, and M. Campillo, Weak Localization of Seismic Waves, Phys. Rev. Lett. **93**, 048501 (2004).
[11] H. Degueldre, J. J. Metzger, T. Geisel, and R. Fleischmann, Random focusing of tsunami waves, Nat. Phys. **12**, 259 (2016).
[12] M. Belzons, E. Guazzelli, and O. Parodi, Gravity waves on a rough bottom: Experimental evidence of one-dimensional localization, J. Fluid Mech. **186**, 539 (1988).
[13] P. Devillard, F. Dunlop, and B. Souillard, Localization of gravity waves on a channel with a random bottom, J. Fluid Mech. **186**, 521 (1988).
[14] P.-E. Wolf and G. Maret, Weak Localization and Coherent Backscattering of Photons in Disordered Media, Phys. Rev. Lett. **55**, 2696 (1985).
[15] F. Wilczek, Quantum Time Crystals, Phys. Rev. Lett. **109**, 160401 (2012).
[16] V. Pacheco-Peña and N. Engheta, Antireflection temporal coatings, Optica **7**, 323 (2020).
[17] A. Akbarzadeh, N. Chamanara, and C. Caloz, Inverse prism based on temporal discontinuity and spatial dispersion, Opt. Lett. **43**, 3297 (2018).
[18] V. Pacheco-Peña and N. Engheta, Temporal aiming, Light **9**, 129 (2020).
[19] A. Shapere and F. Wilczek, Classical Time Crystals, Phys. Rev. Lett. **109**, 160402 (2012).
[20] E. Lustig, Y. Sharabi, and M. Segev, Topological aspects of photonic time crystals, Optica **5**, 1390 (2018).
[21] G. d'Hardemare, A. Eddi, and E. Fort, Probing Floquet modes in a time periodic system with time defects using Faraday instability, Europhys. Lett. **131**, 24007 (2020).
[22] A. Lubatsch and R. Frank, Evolution of Floquet topological quantum states in driven semiconductors, Eur. Phys. J. B **92**, 215 (2019).
[23] S. Fishman, D. R. Grempel, and R. E. Prange, Chaos, Quantum Recurrences, and Anderson Localization, Phys. Rev. Lett. **49**, 509 (1982).
[24] H. Ammann, R. Gray, I. Shvarchuck, and N. Christensen, Quantum Delta-Kicked Rotor: Experimental Observation of Decoherence, Phys. Rev. Lett. **80**, 4111 (1998).
[25] K. Sacha and D. Delande, Anderson localization in the time domain, Phys. Rev. A **94**, 023633 (2016).
[26] D. Delande, L. Morales-Molina, and K. Sacha, Three-Dimensional Localized-Delocalized Anderson Transition in the Time Domain, Phys. Rev. Lett. **119**, 230404 (2017).
[27] Y. Sharabi, E. Lustig, and M. Segev, Disordered Photonic Time Crystals, Phys. Rev. Lett. **126**, 163902 (2021).
[28] R. Carminati, H. Chen, R. Pierrat, and B. Shapiro, Universal statistics of waves in a random time-varying medium, Phys. Rev. Lett. **127**, 094101 (2021).
[29] J. Garnier, Wave propagation in periodic and random time-dependent media, Multiscale Model. Simul. **19**, 1190 (2021).
[30] Y. N. Demkov and V. N. Ostrovskii, *Zero-Range Potentials and their Applications in Atomic Physics* (Springer, New York, 1988).
[31] V. Bacot, M. Labousse, A. Eddi, M. Fink, and E. Fort, Time reversal and holography with spacetime transformations, Nat. Phys. **12**, 972 (2016).
[32] V. Bacot, G. Durey, A. Eddi, M. Fink, and E. Fort, Phase-conjugate mirror for water waves driven by the Faraday instability, Proc. Natl. Acad. Sci. U.S.A. **116**, 8809 (2019).
[33] M. Faraday, On a peculiar class of acoustical figures; and on certain forms assumed by groups of particles upon vibrating elastic surfaces, Phil. Trans. R. Soc. London **121**, 299 (1831).
[34] S. Douady, Experimental study of the Faraday instability, J. Fluid Mech. **221**, 383 (1990).
[35] T. B. Benjamin and F. J. Ursell, The stability of the plane free surface of a liquid in vertical periodic motion, Proc. R. Soc. A **225**, 505 (1954).
[36] V. A. Briskman and G. F. Shaidurov, Parametric excitation of instability of a fluid in magnetic and electric fields, Magn. Gidrodin. Akad. Nauk Lat. SSR **5**, 15 (1969), http://mhd.sal.lv/Download/mydownload.php?ed=p&vol=5&nr=3&an=3&p1=15&p2=10.
[37] C.-S. Yih, Stability of a horizontal fluid interface in a periodic vertical electric field, Phys. Fluids **11**, 1447 (1968).
[38] K. Ward, S. Matsumoto, and R. Narayanan, The electrostatically forced Faraday instability: Theory and experiments, J. Fluid Mech. **862**, 696 (2019).
[39] L. D. Landau and E. M. Lifshitz, *Mechanics* (Pergamon Press, New York, 1969).
[40] K. Kumar and L. S. Tuckerman, Parametric instability of the interface between two fluids, J. Fluid Mech. **279**, 49 (1994).
[41] E. I. Butikov, Parametric excitation of a linear oscillator, Eur. J. Phys. **25**, 535 (2004).
[42] C. Floris, Mean square stability of a second-order parametric linear system excited by a colored Gaussian noise, J. Sound Vib. **336**, 82 (2015).

[43] C. Fang, J. Yang, and X. Liu, Moment Lyapunov exponent of three-dimensional system under bounded noise excitation, Appl. Math. Mech.-Engl. Ed. **33**, 553 (2012).

[44] H. Furstenberg and H. Kesten, Products of random matrices, Ann. Math. Stat. **31**, 457 (1960).

[45] A. Comtet, C. Texier, and Y. Tourigny, Lyapunov exponents, one-dimensional Anderson localization and products of random matrices, J. Phys. A **46**, 254003 (2013).

[46] S. Wildeman, Real-time quantitative Schlieren imaging by fast Fourier demodulation of a checkered backdrop, Exp Fluids **59**, 97 (2018).

[47] F. Pétrélis, S. Aumaître, and S. Fauve, Effect of Phase Noise on Parametric Instabilities, Phys. Rev. Lett. **94**, 070603 (2005).

[48] K. Ramola and C. Texier, Fluctuations of random matrix products and 1D Dirac equation with random mass, J. Stat. Phys. **157**, 497 (2014).

[49] L. S. Froufe-Pérez, M. Engel, J. J. Sáenz, and F. Scheffold, Band gap formation and Anderson localization in disordered photonic materials with structural correlations, Proc. Natl. Acad. Sci. U.S.A. **114**, 9570 (2017).